Engineering Science and Technology, an International Journal 19 (2016) 1177–1189

HOSTED BY

Contents lists available at ScienceDirect

Engineering Science and Technology, an International Journal

journal homepage: http://www.elsevier.com/locate/jestch

Full Length Article

Effect of wall proximity of two staggered triangular cylinders on the transport process in a channel

Mousa Farhadi *, Kurosh Sedighi, Afshin Mohsenzadeh Korayem

Faculty of Mechanical Engineering, Babol University of Technology, Babol, Islamic Republic of Iran

ARTICLE INFO

Article history:
Received 8 September 2015
Received in revised form
12 February 2016
Accepted 12 February 2016
Available online 23 March 2016

Keywords:
Unsteady laminar flow
Force convective heat transfer
Staggered triangular cylinders
Wall proximity

ABSTRACT

A numerical investigation has been carried out to analyze the heat transfer and the flow field around two isothermal triangular cylinders of equal size placed staggered in a horizontal plane channel with adiabatic walls. Computations have been carried out for Reynolds numbers (based on triangle width) 100, 250, and 350, lateral gap ratios (d/B) 0, 0.5, and 1, and longitudinal gap ratios (S/B) 1, 2, 3 and 4. The effect of longitudinal and lateral gap between obstacles and proximity of channel walls is investigated. Results show that when obstacles are placed in close vicinity of the channel's wall (d/B = 1), vortex shedding disappears at the downstream of triangles at Re = 100 and 250 at all S/B, but for Re = 350 creating and disappearing of the vortex shedding depend on the longitudinal gap ratio (S/B). Proximity of obstacles has more effect on the second triangle than the first triangle especially from longitudinal gap ratio equals 2, so that with approaching the channel wall, the Nusselt number for the first triangle decreases, while for the second triangle a different behavior is seen. Staggered arrangement causes the Nusselt number of the second triangle to become greater than the first triangle.

1. Introduction

Staggered arrangement of obstacles has been always one of the points of interest in heat transfer and fluid mechanic field. It is perhaps because of decreasing drag coefficient and increasing heat transfer. Wang et al. [1] studied drag reduction of a circular cylinder experimentally while a rod was placed upstream of the cylinder. They showed that the upstream rod can reduce the resultant force of the cylinder at various spacing between the rod and the cylinder for $\alpha < 5^\circ$ (α defined as the staggered angle of the rod and the cylinder), but for $\alpha > 10^\circ$ upstream rod cannot reduce the force on the cylinder any more. Zhang et al. [2] studied square cylinder with an upstream rod in a staggered arrangement. They found six different flow modes with various staggered angles and spacing ratios. Molki and Fotouhi [3] investigated the laminar forced convection heat transfer from a circular cylinder numerically. The results showed that the periodic nature of eddies causes an oscillatory behavior in the heat transfer coefficients. Sumner et al. [4] studied vortex shedding for different gap spaces and staggered angle, and they found that the behavior of the Strouhal number depends on the space of the circular cylinders. Dey and Das [5] investigated the drag and lift reduction on square cylinder with triangular solid numerically. The effect of triangular length and inclination angle on drag and lift coefficients was studied. Akbari and Price [6] studied flow patterns around two staggered circular cylinders in cross-flow at Re = 800. They found five distinct flow regimes, depending on pitch ratio and staggered angle. Matos et al. [7] studied staggered finned circular and elliptic tubes. They showed that the elliptical tube arrangements have better overall performance and lower cost than the traditional circular tube geometry. Ghosh et al. [8] investigated forced convective heat transfer over a bank of staggered cylinders. They showed that the rates of heat transfer between the fluid and the staggered cylinders are affected by both the Reynolds number and cylinder spacing.

The flow of fluids past bluff bodies such as square and circular cylinders occurs in many industrially important applications [9]. One of the basic configurations that can be also used as a bluff body is a triangular obstacle [10–16]. By reviewing the literature, it reveals that it has not been studied enough especially in the heat transfer field. Buresti et al. [10] carried out an experimental investigation for triangular prisms with two different cross sections (i.e. equilateral and isosceles with 90° apex angle). They tried to find the critical aspect ratio that below it vortex shedding shifts from alternate type (i.e. the usual Karman alternate shedding of vortices from the two sides of the body) to the second type of shedding (i.e. a symmetrical shedding of "arch-type" vortices). But just alternate vortex shedding was found for all aspect ratios. Csiba and Martinuzzi [11]

* Corresponding author. Tel.: +98 111 3234205, fax: +98 111 3212268.
E-mail address: mfarhadi@nit.ac.ir (M. Farhadi).
Peer review under responsibility of Karabuk University.

http://dx.doi.org/10.1016/j.jestch.2016.02.005
2215-0986/

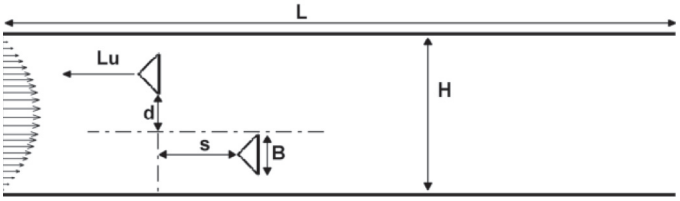

Fig. 1. Geometry of problem.

Table 1
Results of grid dependence.

Grid	Δx_{min}, Δy_{min}	$\langle \overline{Nu} \rangle$ first obstacle	$\langle \overline{Nu} \rangle$ second obstacle
187×68	0.023B	5.31	6.56
215×89	0.014B	5.52	6.81
215×100	0.012B	5.65	6.90
230×110	0.008B	5.7	6.93

investigated experimentally the influence of the incidence angle of the Strouhal number of an isosceles triangle. They showed that when the Strouhal number is defined based on the triangle width (B), the Strouhal number increases with incidence angle, α, but when the Strouhal number is defined based on $B' = B\cos\alpha$ as a length scale, Strouhal number is independent of α. The laser Doppler velocimetry (LDV) study of Ulrichs and Herwig [12] over a right-angled triangle about the separation behavior of bluff bodies in the vicinity of a wall showed that when the triangle is placed in the vicinity of the wall there will be two separate regions: (i) bluff body separation region and (ii) wall bounded separation region. As the triangle moves away from the wall, the wall bounded separation region eventually disappears. Abbassi et al. [14] carried out a numerical investigation to study forced convection of air for a two-dimensional

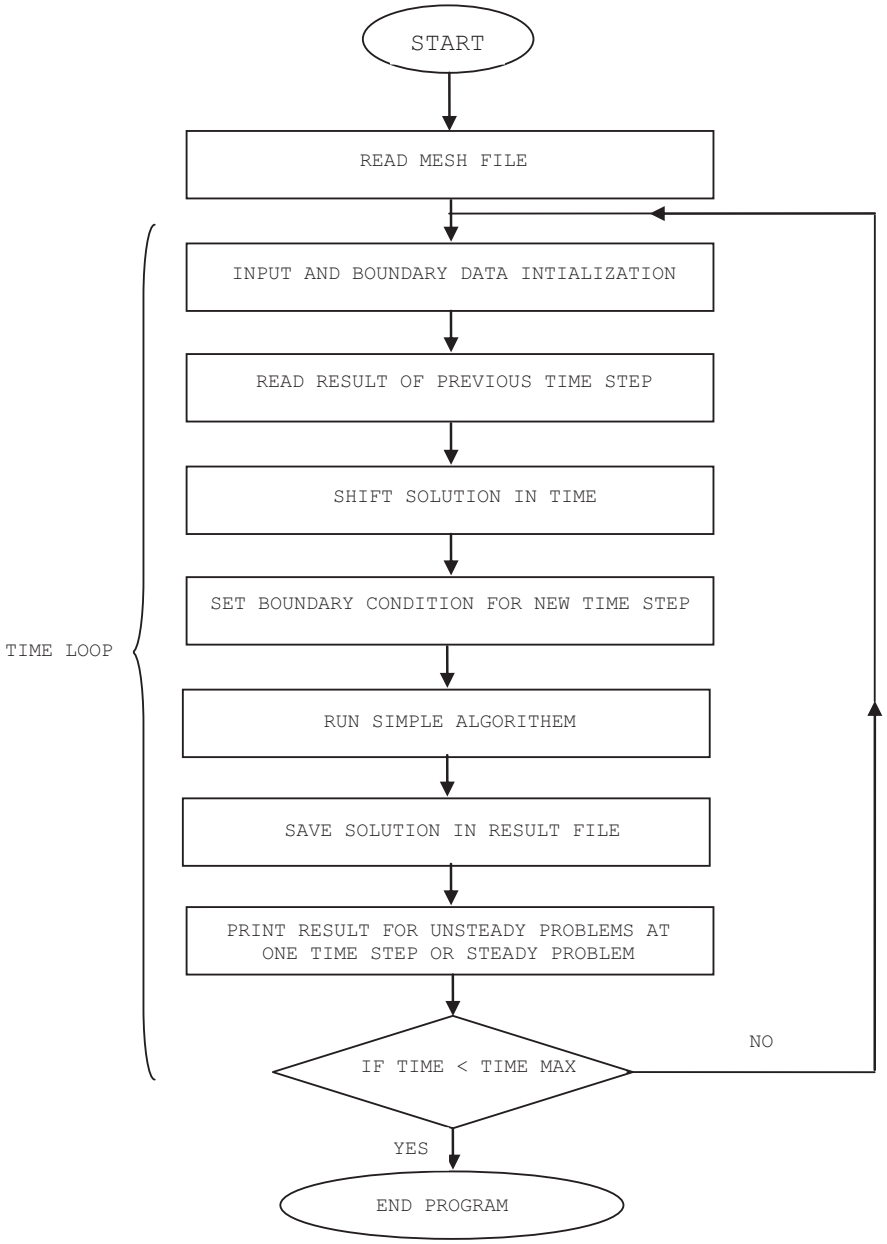

Fig. 2. Simple algorithm of the UTFN code.

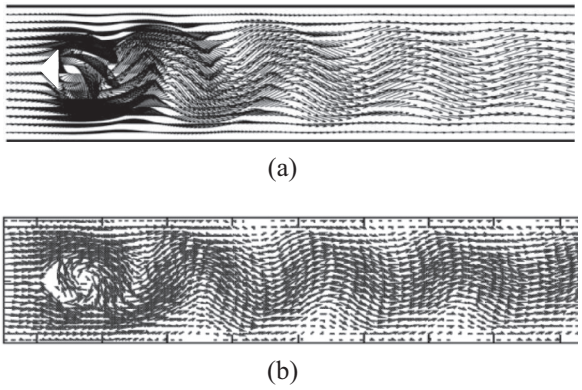

Fig. 3. The instantaneous vectors plot of (a) the present study and (b) Abbassi et al. [14].

unsteady-laminar flow in a horizontal channel with a built-in triangular prism. They showed that the presence of triangular prism for symmetric flow (Re < 45) has just a little local effect on heat transfer from the channel wall. In contrast, in the periodic flow (Re ≥ 45), the presence of triangular prism has an important effect in enhancement of heat transfer from the channel wall. Chattopadhyay [15] studied the same geometry but for turbulence flow. In this case an augmentation of about 17% in averaged Nusselt number is recorded. Wang et al. [17] investigated the interaction of two freely rotatable triangular cylinders that are placed in tandem in a laminar flow numerically. Tu et al. [18] studied the effect of a stationary and rotationally oscillating equilateral triangular cylinder on flow field numerically. They investigated the variable incident angle, Reynolds number, oscillating amplitude, and oscillating frequency. Ghafouri et al. [19] studied the deposition and dispersion of particles with size of μm in a channel over a triangle obstacle by lattice Boltzmann method. They investigated the effect of all forces on particle motion, such as Brownian, gravity, drag and lift forces. Agrwal et al. [20] investigated the flow field behind triangular prisms at intermediate Reynolds number with different apex angles experimentally. They reported that a linear relationship exists between vortex shedding frequency and apex angle. On the other hand they observed a minimum drag coefficient and a maximum Strouhal number for an apex angle of 30 degrees.

On the other hand the effect of wall proximity of obstacles on flow field and heat transfer also has been investigated by researchers [16,21–29]. When obstacles are placed close to the wall in an asymmetric arrangement, for sufficient small gap between obstacle and channel wall, G, flow become suppress and vortex shedding disappears. This critical gap depends on the boundary layer thickness (δ/D) and Reynolds number. Different critical values for the gap between obstacle and channel wall at high Reynolds numbers have been reported by authors. An LDV research by Durao et al. [21] on a square cylinder showed that vortex shedding is suppressed at G/D = 0.35 for Re = 13,600 and δ/D = 0.8. Bosch et al. [22] suggested critical gap height of G/D = 0.35 at Re = 22,000, δ/D = 0.13. For a circular cylinder, boundary layer thickness has an important role in gap height unlike square cylinder. The different relation between the boundary layer thickness and gap height has been reported by Lei et al. [23]. They reported that as boundary layer thickness increases from 0.14 to 0.29, a critical gap height decreases from 0.4 to 0.2, whereas Grass et al. [24] suggested a direct relation between the boundary layer thickness and critical gap height. They reported that boundary layer thickness (δ/D) increases from 0.28 to 6 when the critical gap height varies from 0.25 to 0.5.

Chakrabarty and Brahma [25,26] carried out an experimental investigation into the effect of wall proximity on heat transfer and flow field around a square [25] and rectangular [26] prism for the Reynolds number 4.9×10^4, different blockage ratios, aspect ratios, height ratios and various angles of attack. They observed that the drag coefficient and the local Nusselt number for all blockage ratios and angles of attack decrease as the prism approaches the upper wall. Fohanno and Polidori [16] investigated the effects of the gap size in the start-up free convective flow around a square prism near a wall with changing the gap, *G*, between the prism and the wall from G = 0 to $G \to \infty$. They showed that the reduction of the gap height, $G/D \leq 0.1$, reveals more complex flow patterns due to the increase of the adverse pressure gradient leading to the separation of the viscous layer downstream of the prism. Singha et al. [27] carried out a numerical investigation into the effect of wall proximity on heat transfer and flow field around a circular cylinder for the Reynolds number between 200 and 250 and gap height, G/D, between .1 and 2.5. They found that as cylinder approaches the wall, vortex shedding regime from two rows of vortices of opposite-sign changes to single row vortices of same-sign. Flow also becomes suppressed under the critical gap height. Rosales et al. [28] studied numerically a tandem pair of squares of unequal sizes (i.e. eddy square that is adiabatic and heated square) in channel flow at Re = 500 and longitudinal gap space equals 2 based on side length of the heated cylinder. They investigated the effect of wall proximity of obstacle on heat transfer from heated obstacle and flow field in in-line and staggered position. They showed that the drag coefficient, Strouhal number and Nusselt number of the cylinder decrease as the heated cylinder approach the wall. Mohsenzadeh et al. [29] studied the effect of wall proximity of two in-line triangular cylinder at Re = 100, 250 and 350. They show that when cylinders are placed at close proximity of channel wall, G/B = 0.5, from S/B = 1 to 3, vortex shedding is removed at the downstream of the second triangle, but at S/B = 4, vortex shedding is created at Re = 250 and 350. Other studies were only done for flow and heat transfer over a single triangular cylinder recently [30–33].

The goal of this study is to understand the effect of cylinder's wall proximity, longitudinal and lateral space of cylinders on flow structures, and fundamental mechanisms of vortex formation. Results are presented at Re = 100, 250, and 350, longitudinal gap ratios (S/B) equals 1, 2, 3, and 4, and the lateral gap ratio (d/B) equals 0, 0.5, and 1. Results for in-line arrangement are also presented for comparison with staggered arrangement.

Table 2
Comparison $\langle \overline{Nu} \rangle$ between the present work with the previous numerical study [14].

Re	Present study	Abbassi et al. [14]
30	0.71	0.68
100	1.58	1.44
150	2.06	1.96
250	2.62	2.51

Table 3
Comparison between the present work with the previous numerical study [35] of flow over a square cylinder.

Geometry	C_D		St	
	Present study	Sohankar et al. [35]	Present study	Sohankar et al. [35]
Square cylinder at α = 0 and Re = 100	1.447	1.444	1.40	1.45
Square cylinder at α = 45 and Re = 200	1.901	1.944	0.195	0.204

2. Governing equation

The flow is assumed unsteady, two-dimensional and laminar, for which the governing conservation equations of mass, momentums and energy can be written in the following forms:

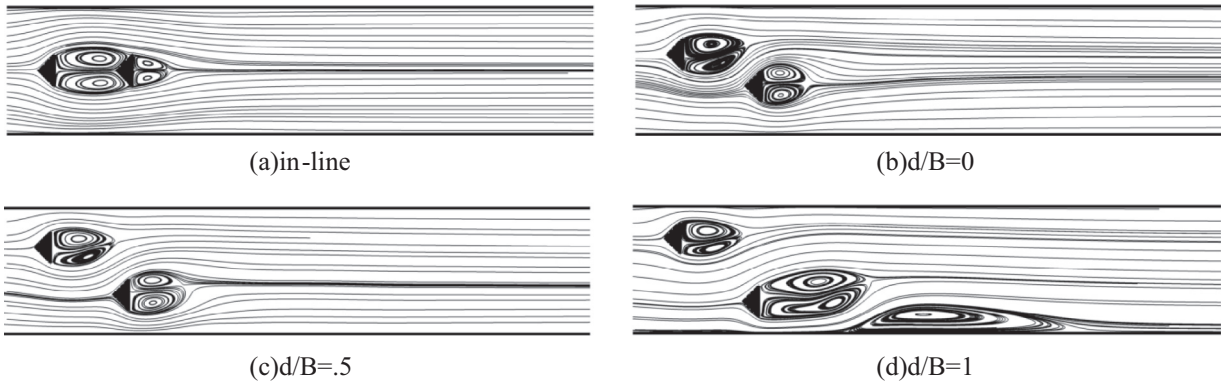

Fig. 4. Time-averaged streamlines for in-line and staggered arrangement at S/B = 2 and Re = 250.

$$\frac{\partial u}{\partial x}+\frac{\partial v}{\partial y}=0 \tag{1}$$

$$\frac{\partial u}{\partial \tau}+\frac{u\partial u}{\partial x}+\frac{v\partial u}{\partial y}=-\frac{\partial P}{\partial x}+\frac{1}{\mathrm{Re}}\left(\frac{\partial^2 u}{\partial x^2}+\frac{\partial^2 u}{\partial y^2}\right) \tag{2}$$

$$\frac{\partial v}{\partial \tau}+\frac{u\partial v}{\partial x}+\frac{v\partial v}{\partial y}=-\frac{\partial P}{\partial y}+\frac{1}{\mathrm{Re}}\left(\frac{\partial^2 v}{\partial x^2}+\frac{\partial^2 v}{\partial y^2}\right) \tag{3}$$

$$\frac{\partial \theta}{\partial \tau}+\frac{u\partial \theta}{\partial x}+\frac{v\partial \theta}{\partial y}=\frac{1}{\mathrm{Re}\cdot\mathrm{Pr}}\left(\frac{\partial^2 \theta}{\partial x^2}+\frac{\partial^2 \theta}{\partial y^2}\right) \tag{4}$$

In the above equations, u, v, θ, P, Re and Pr are dimensionless fluid velocities, temperature, pressure, Reynolds number and Prandtl number (Pr = 0.71) respectively. The dimensionless forms of the variables are:

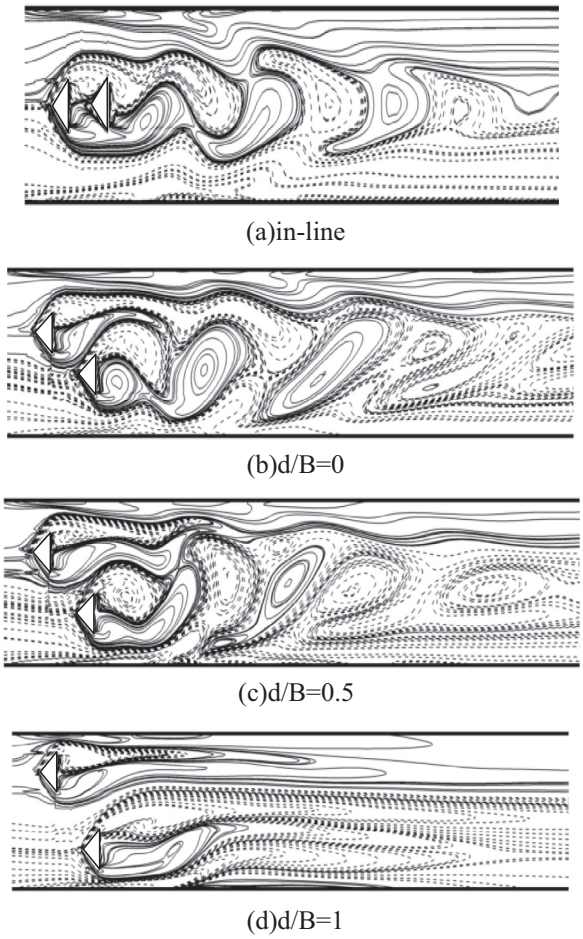

Fig. 5. Instantaneous vorticity contours (Wz) for different lateral gap ratios (d/B) at S/B = 1 and Re = 250.

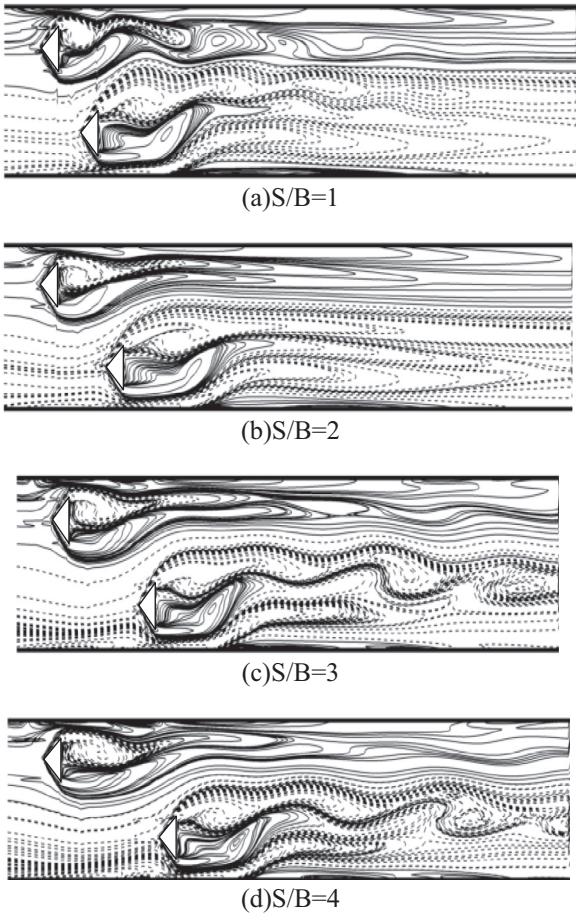

Fig. 6. Instantaneous vorticity contours (Wz) for different longitudinal gap ratios (S/B) at d/B = 1 and Re = 350.

$$x=\frac{x^*}{B},\quad y=\frac{y^*}{B},\quad \tau=\frac{tu^*_{\max}}{B},\quad u=\frac{u^*}{u^*_{\max}},\quad v=\frac{v^*}{u^*_{\max}},$$
$$P=\frac{P^*}{\rho u^{*2}_{\max}},\quad \theta=\frac{T-T_C}{T_H-T_C} \tag{5}$$

The thermal heat flux exchanged between the obstacles and the flow is specified by the streamwise-averaged Nusselt number calculated as follows:

$$\overline{Nu}=\frac{1}{l/B}\int_o^{l/B} Nu\,dl \tag{6}$$

where Nu is the local Nusselt number, which is defined as:

$$Nu=-\partial\theta/\partial n\big|_{n=0} \tag{7}$$

The streamwise- and time-averaged Nusselt number is defined as:

$$\langle\overline{Nu}\rangle=\frac{1}{t_1}\int_o^{t_1}\overline{Nu}\,dt \tag{8}$$

where t_1 is the total time.

3. Computational domain and boundary condition

The computational domain is shown in Fig. 1. Geometry considered is a horizontal plane channel with two staggered isosceles triangles of equal size with 90° apex angle. The distance between two cylinders is "***d***." The dimensionless channel length is (L/B > 24) and the upstream distances, 'Lu', is selected as 4B. The triangle bottom width (B) was selected as H/4, which corresponds to the blockage ratios of 0.25.

The longitudinal gap ratio (S/B) and lateral gap ratio (d/B) are changeable [(S/B = 1, 2, 3, 4), (d/B = 0, 0.5, 1)]. Results for in-line arrangement are also presented for comparison with staggered arrangement.

At the channel inlet, the local normal component of velocity is assumed to be zero, and a fully developed parabolic profile for the axial velocity prescribed:

$$u^*=u^*_{\max}\left(1-\left(\frac{y^*}{y^*_B}\right)^2\right),\quad v^*=0 \tag{9}$$

where u^* and v^* are local components of velocity, and y^*_B = h., and the incoming stream is assumed to be in a constant temperature T_C, while the triangular obstacles are at a temperature T_H that $T_H > T_C$.

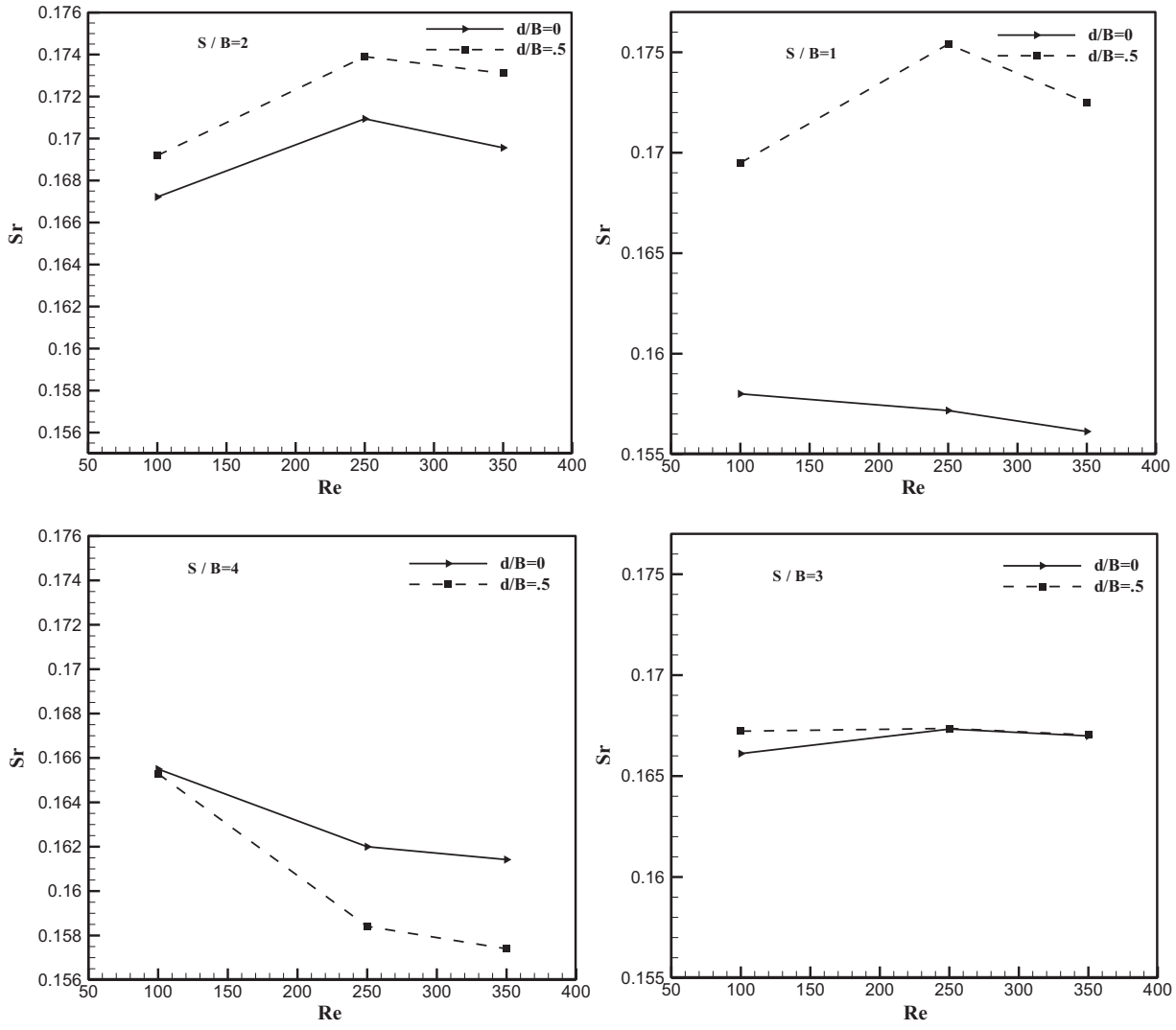

Fig. 7. Variation of Strouhal number with Reynolds number for different lateral gap ratios (d/B) at constant S/B.

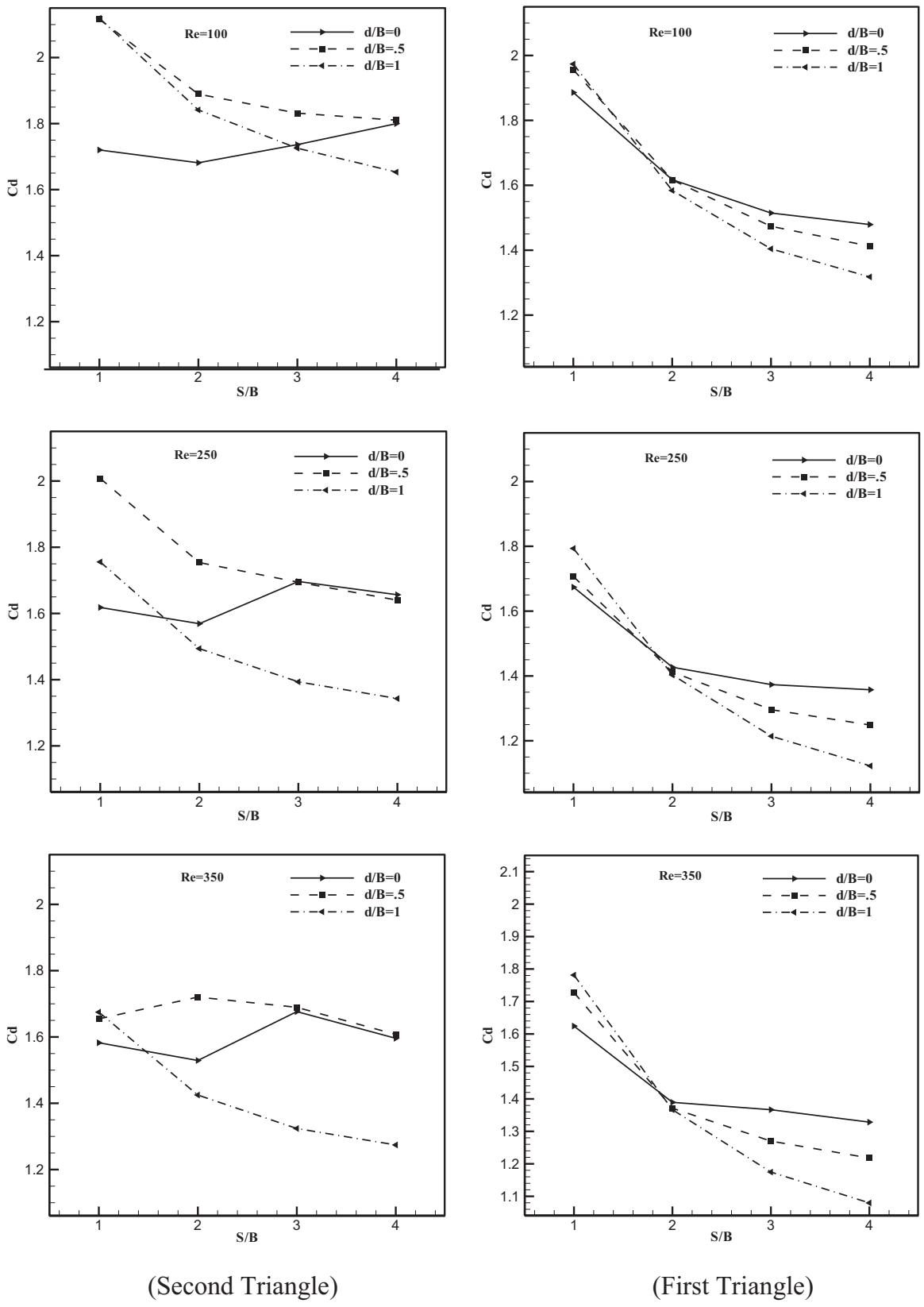

Fig. 8. Variation of drag coefficient with longitudinal gap ratio (S/B) for different lateral gap ratio (d/B) at constant Reynolds numbers.

The bottom and top walls of the channel are adiabatic. No-slip boundary conditions for the velocity are imposed on the upper and lower channel walls and the cylinder surfaces. At outlet the Convective Boundary Condition (CBC) is as follows:

$$\frac{\partial \phi}{\partial \tau} + U \frac{\partial \phi}{\partial X} = 0 \tag{10}$$

In the above equation, ϕ is any of the dependent variables and U is a mean dimensionless velocity on the outflow.

4. Numerical procedure and validation

The mentioned equations in the previous section are solved by UTFN (Unsteady Turbulent Flow at Non-orthogonal coordinates) code, which is a computer code for computation of two dimensional steady/unsteady and turbulent/laminar flows in FORTRAN. The finite volume method is applied to transfer the partial differential equations to algebraic relations. Then the SIP (Strongly Implicit Procedure) [34] Algorithm is used to solve the obtained algebraic equations. The present code utilizes the collocated variable arrangement and uses Cartesian velocity components in which all variables are stored at the same control volume. In order to solve the Navier–stokes and continuity equations the SIMPLE method supplying the pressure–velocity coupling is used. This method has its origin in staggered grid methodology and is adapted to collocated grid methodology through the use of Rhie and Chow interpolation [34]. This interpolation can increase the stability of solution too. The unsteady term is discretized by a three time level method. In addition three different discretization schemes are available to approximate the convective terms, Upwind/Central Difference and Hybrid schemes. Diffusion term is discretized by CDS. In this study, The Convection and Diffusion terms of the equations are discretized by Central Difference Scheme (CDS). The simple algorithm of the computer program is shown in Fig. 2. Further details about the numerical method are given in Farhadi et al. [30].

A non-uniform grid that is non-orthogonal before the obstacles is used with a minimum spacing near the sides of the obstacle and stretching with the fix factor. To check grid independence in this work, one case was Run (S/B = 3, d/B = 0.5) for Re = 350. Table 1 shows the results of grid independency for time and space-averaged Nusselt number. Results show that, when the number of grid points passes from a 187×68 to 215×89, the space and time-average Nusselt number increase 4% and 3.8% for the first and second triangle, respectively, and when the number of grid points passes from

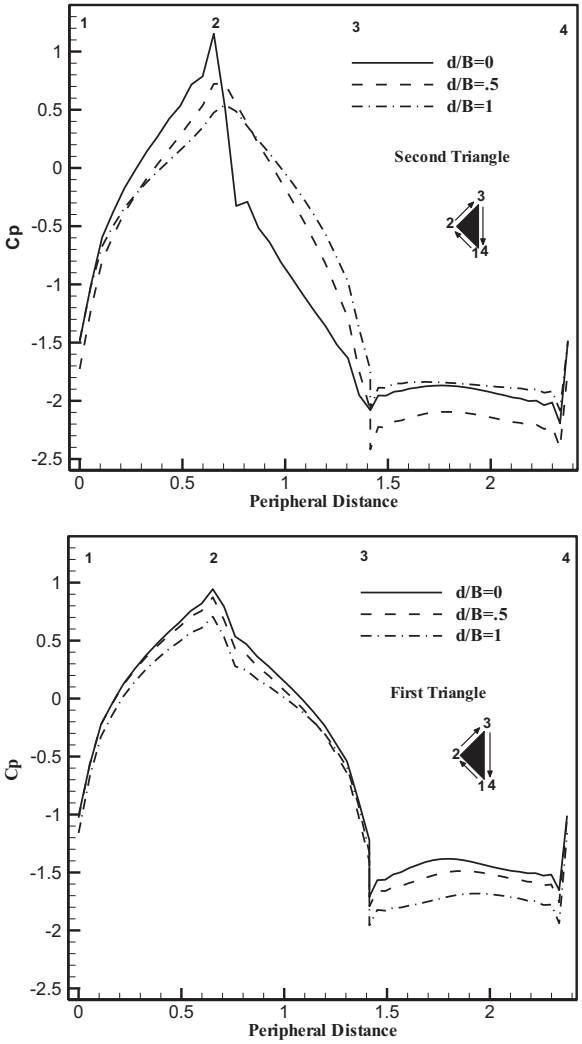

Fig. 9. Pressure coefficient, C_P, distribution over the triangles' surface at S/B = 1 and Re = 250.

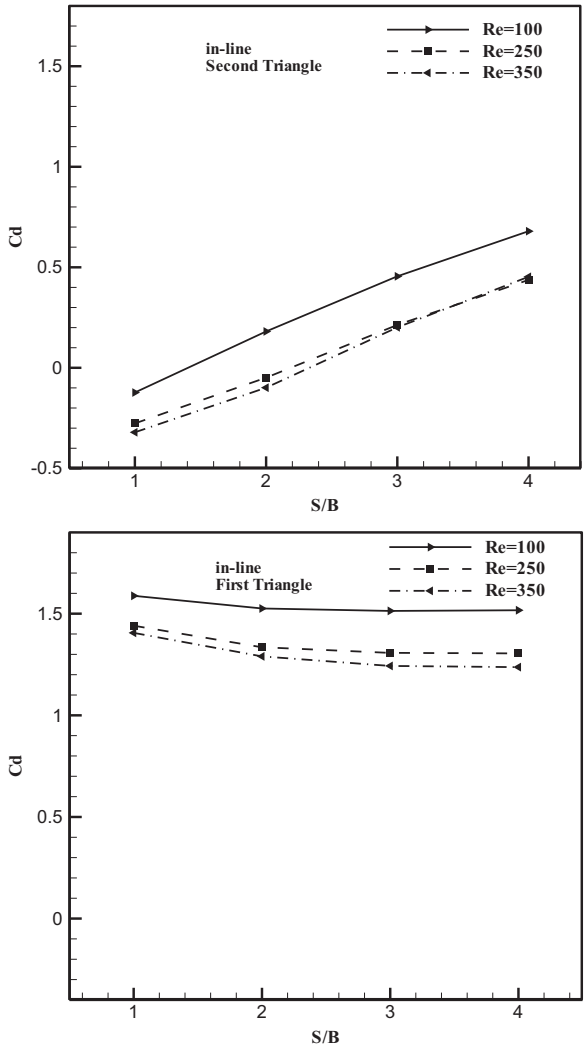

Fig. 10. Variation of drag coefficient with longitudinal gap ratio (S/B) for different Reynolds numbers in in-line arrangement.

a 215 × 89 to 215 × 100, it increases 2.3% and 1.3%. But when the number of grid points passes from 215 × 100 to 230 × 110, it increases only 0.88% and 0.43%. These grid points have a minimum grid spacing 0.0231B, 0.014B, 0.012B and 0.008B for 187 × 68, 215 × 89, 215 × 100 and 230 × 110, respectively. Therefore the minimum grid spacing 0.012B is sufficient and is retained for other investigations.

This case corresponds to the work of Abbassi et al. [14]. The instantaneous vectors pattern for Re = 100 was presented and compared with the result of Ref. [14] in Fig. 3. This figure shows a good agreement of present data in comparison with other numerical result. Table 2 shows the time and streamwise-averaged Nusselt number over the lower wall of the channel. A good agreement between the results of this work and the previous study can be observed. For better validation of the UTFN code, the flow over a square cylinder at incidence was studied in the free stream flow. The results of the present work were compared with the previous published work (Sohankar et al. [35]), which is shown in Table 3. The results show a good agreement in comparison with Ref. [35].

5. Results

5.1. Flow field

In this part the effects of the Reynolds number, lateral gap ratio (d/B) and longitudinal gap ratio (S/B) over the flow field and flow characteristic such as the drag coefficient and Strouhal number were investigated. Fig. 4 shows the time-averaged streamlines for in-line and staggered arrangement at different lateral gap ratios (d/B = 0, 0.5, 1) at S/B = 2 and Re = 250. It is observed that a circulation zone is formed along the lower wall of the channel downstream of the second triangle at d/B = 1. Such a behavior is also seen in other Reynolds number at d/B = 1 for all longitudinal gap ratio from S/B = 1 to 4.

The position of obstacles in wall proximity is also effective over the formation of vortex. Fig. 5 shows instantaneous vorticity contours for in-line and staggered arrangement at different lateral gap ratios (d/B = 0, 0.5, 1) at S/B = 1 and Re = 250. By approaching the wall vortex shedding is removed at d/B = 1 for Re = 100 and 250. This phenomenon is again seen for all (S/B) from 1 to 4. But there is a different behavior at Re = 350 and d/B = 1 with increasing longitudinal gap ratio (S/B). When obstacles are placed at position S/B = 1 and d/B = 1, vortex shedding is created at Re = 350 downstream of the first cylinder, unlike Re = 100 and 250, while as obstacles are placed at position S/B = 2 and d/B = 1, vortex shedding is removed at Re = 350 like Re = 100 and 250 and unlike S/B = 1; on the other hand, for position S/B = 3 and d/B = 1 vortex shedding is created at Re = 350, but unlike S/B = 1 this time vortex shedding is seen downstream of the second triangle while at S/B = 1 vortex shedding is created downstream of the first triangle. The same behavior as S/B = 3 is seen at S/B = 4. Fig. 6 shows how vortex shedding is created and removed with increasing longitudinal gap ratio (S/B) at d/B = 1 and Re = 350.

The Strouhal number is investigated to consider the frequency of vortex shedding. Fig. 7 shows the variation of the Strouhal number (Sr) with Reynolds number for different longitudinal and lateral gap ratios. As mentioned before when obstacles are placed at position d/B = 1, vortex shedding is suppressed for Re = 100 and 250 at all S/B, which is due to damping effect of channel's wall on flow, so that Strouhal number becomes zero in these positions; on the other hand, when obstacles are placed at d/B = 0, the proximity of two obstacles has a quite the same effect as the channel's wall on flow and vortex shedding, but for d/B = 0.5 the effect of obstacle's proximities and channel's wall is balanced together, so from S/B = 1 to 3 Strouhal number for d/B = 0.5 is greater than d/B = 0, although at S/B = 3 they become so close to each other at Re = 250 and 350. Finally at S/B = 4 the effect of obstacle's proximity disappears and Strouhal number for d/B = 0 becomes greater than d/B = 0.5.

One of the main parameters affected by the wall and obstacles proximity and also the longitudinal gap ratio is the drag coefficient. With increasing longitudinal gap ratio (S/B), wall proximity has different effects on the drag coefficient of the first and second triangles. Fig. 8shows the variation of the drag coefficient with longitudinal gap ratio (S/B) for different lateral gap ratios (d/B) at constant Reynolds numbers. For S/B = 1 the drag coefficient of both obstacles at d/B = 0 is smaller than d/B = 0.5 and 1. It is because the proximity of two obstacles greatly affects the distribution of pressure drag along the upper side of the second triangle and also the rear side of the first triangle. Fig. 9 shows the variation of pressure coefficient, C_p, over the triangle's surface at S/B = 1 and Re = 250. With increasing S/B, the effect of obstacle proximity on pressure drag becomes less important and the effect of wall's proximity on drag coefficient at d/B = 1 becomes more important especially for the first triangle, so unlike S/B = 1, from S/B = 2 onward the drag coefficient at d/B = 0 begins to increase in comparison with d/B = 0.5 and 1. Drag coefficients for in-line arrangement are shown in Fig. 10, for comparison with the staggered arrangement (Fig. 8).

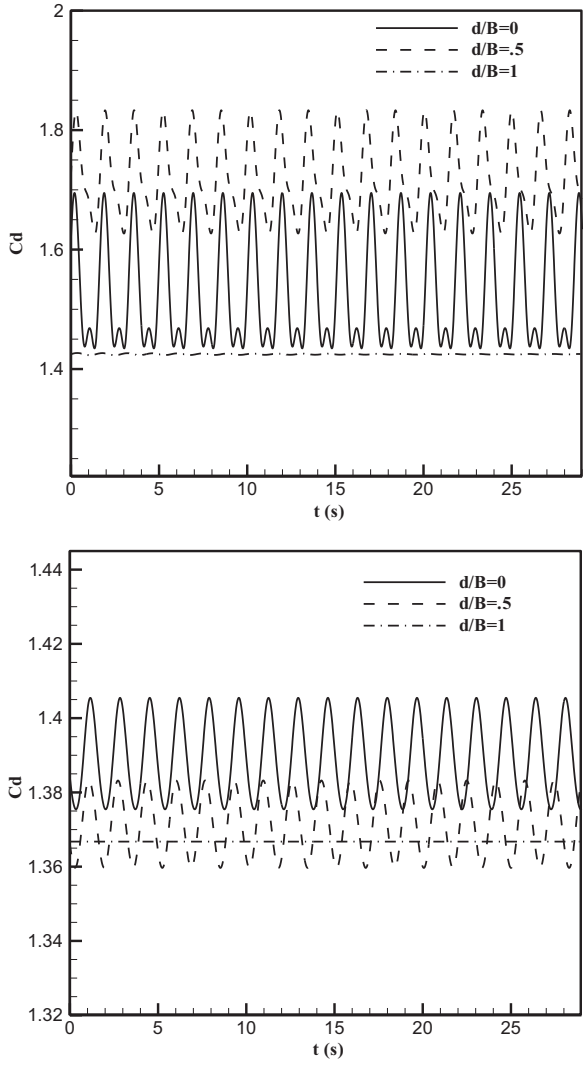

Fig. 11. Instantaneous drag coefficient for different lateral gap ratios at S/B = 2 and Re = 350: second triangle (left), first triangle (right).

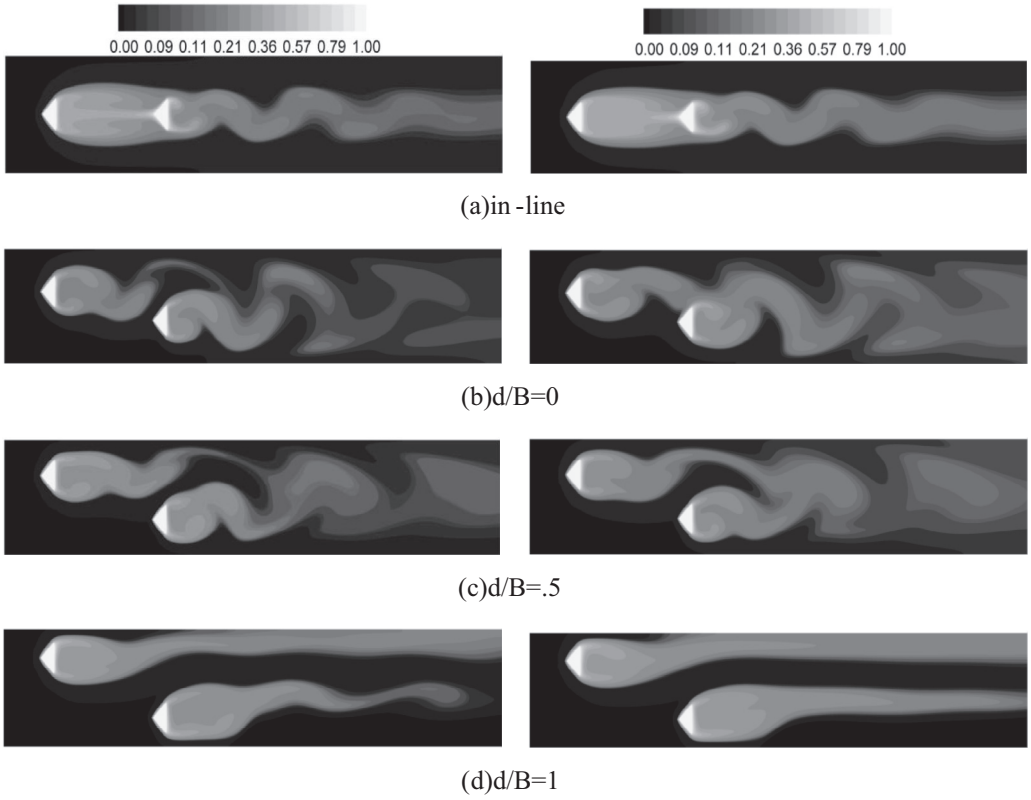

Fig. 12. Instantaneous temperature contours for in-line and staggered arrangement at S/B = 4 for Re = 350 (left) and Re = 250 (right).

Instantaneous drag coefficients for three different lateral gap ratios at Re = 350 and S/B = 2 are shown in Fig. 11. As mentioned before with approaching the wall vortex shedding is removed at d/B = 1, so the variation of drag coefficient with time becomes constant unlike d/B = 0 and 0.5.

5.2. Heat transfer

In this part the effects of gap spacing, wall proximity and Reynolds number on the convective heat transfer over the triangles are investigated. Instantaneous temperature contours for S/B = 4 at Re = 250 and 350 are shown in Fig. 12. When obstacles exit from in-line arrangement, the locked recirculation region between the triangles disappears. Fig. 12 shows how disappearing vortex shedding at downstream of obstacles for position d/B = 1 influences the temperature field at Re = 250 (see Figs. 12d and 5d).

On the other hand at d/B = 1 and Re = 350, with increasing longitudinal gap ratio (S/B), a different behavior was seen downstream of the triangles (see Fig. 6). The effect of this different behavior on temperature field is also shown in Fig. 13.

The time-averaged local Nusselt number distribution over the triangle surfaces is plotted in Figs. 14 and 15. In Fig. 14, the time-averaged local Nusselt number distribution over the second triangle surface at S/B = 1 for in-line and staggered arrangement (d/B = 1) has been compared. A different behavior is seen for the second triangle in in-line and staggered arrangements. It is because at staggered arrangement velocity boundary layer begins at the apex of the triangle so local Nusselt number at this point is greater than the other point around it, but for the second triangle the boundary layer ends at the apex of the triangle.

In Fig. 15, the effects of lateral gap ratio at S/B = 2 and Re = 250 on the distribution of local Nusselt number are shown. As

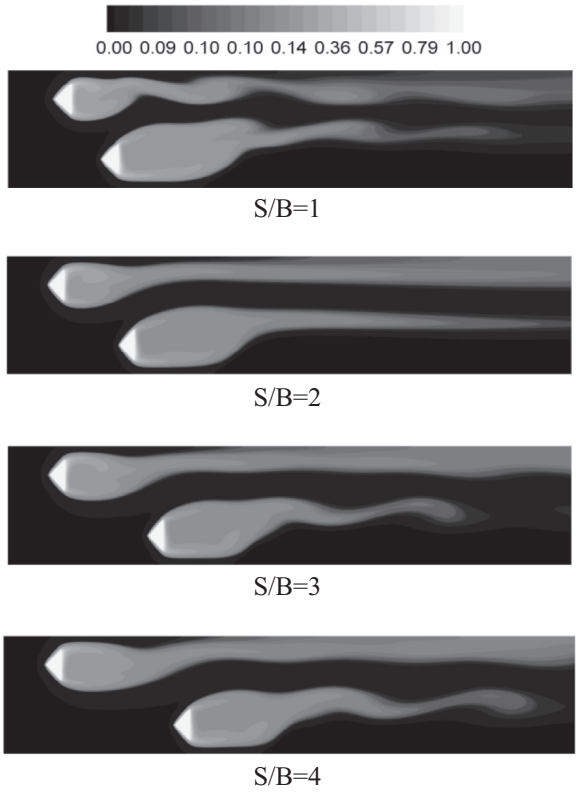

Fig. 13. Instantaneous temperature contours for different longitudinal gap ratios (S/B) at d/B = 1 and Re = 350.

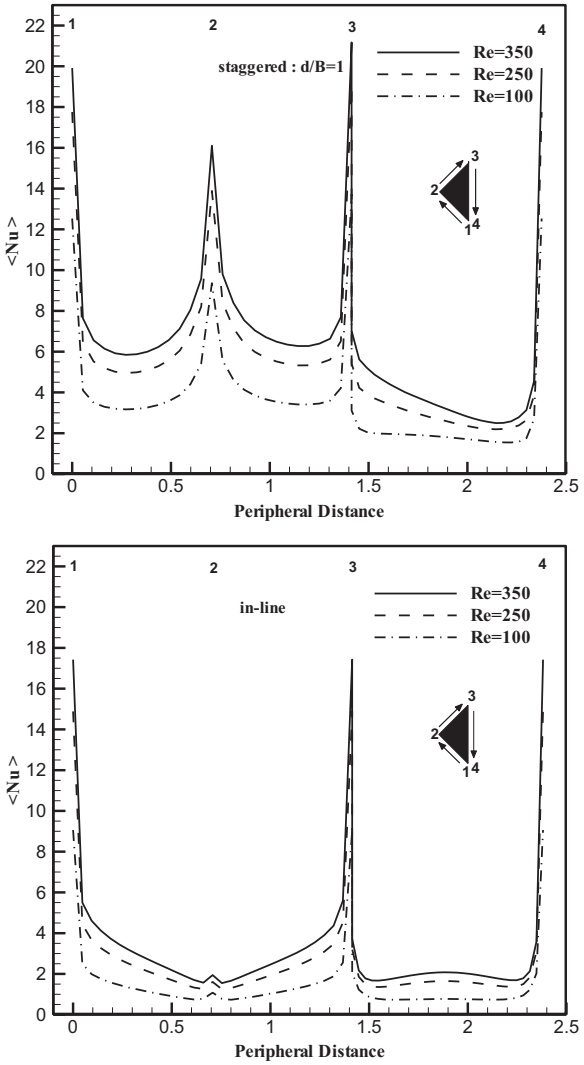

Fig. 14. Time-averaged local Nusselt number distribution over the second triangle surface at in-line (right) and staggered (left) arrangement (d/B = 1) for different Reynolds number at S/B = 1.

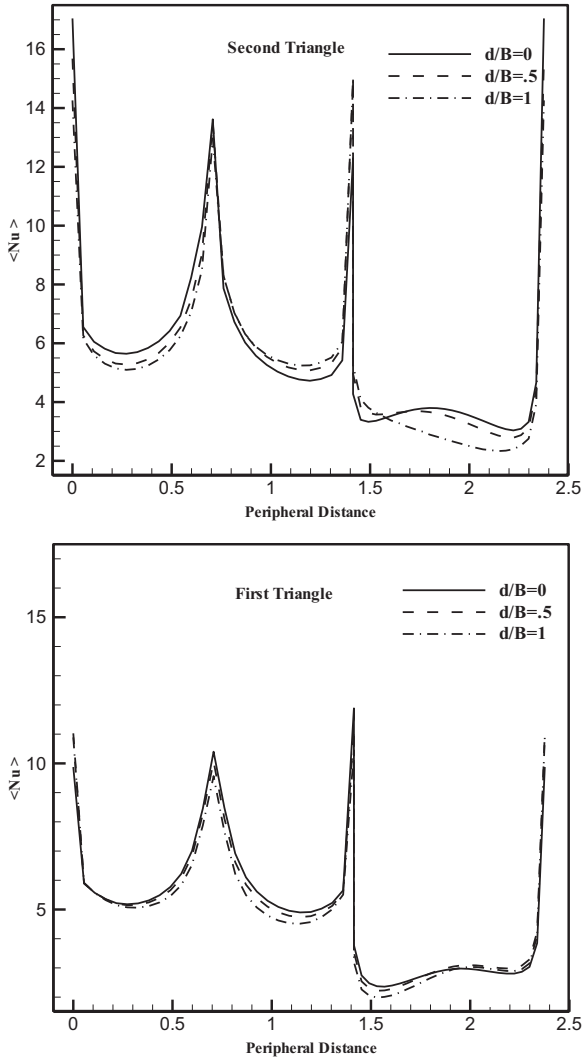

Fig. 15. Time-averaged local Nusselt number distribution over the triangle surface for different d/B at Re = 250 and S/B = 2.

obstacles approach the wall, local Nusselt number at the lower side of the second triangle decreases, while it increases at the upper side. It is because with approaching the wall, the passage between two obstacles becomes larger and more momentum can pass from it, while the passage between the obstacle and channel wall decreases. Such a condition causes the local Nusselt number at the upper side of the first triangle to become smaller than the lower side of it. It should be mentioned that the effect of variations of passage between two obstacles on the first triangle is not as important as the second triangle and the proximity of the two obstacles is more important for the second triangle.

The effect of longitudinal and lateral gap space between obstacles on heat transfer is shown in Fig. 16. For the first triangle, at all longitudinal gap ratio (S/B), with approaching the wall, Nusselt number decreases, but for the second triangle Nusselt number at d/B = 0.5 is maximized. When the second triangle is placed at d/B = 0, although it is far away from the channel wall, it is in close vicinity of the first triangle, and the first triangle has a quite the same effect like the channel on the second triangle; on the other hand, when the second triangle is placed at position d/B = 1, it is affected by channel wall. But at d/B = 0.5, the second triangle is placed in a balanced situation in relation to the channel wall and first obstacle. In other words, the passage between the second triangle and first triangle in one hand, and the passage between the second triangle and lower channel wall on the other hand, are placed in a quite equal size, and a quite balanced momentum passes from them unlike d/B = 0 and 1. The other important point that should be mentioned is that the proximity of the two obstacles affects more the second triangle than the first triangle, and the first triangle is affected more by the channel wall (see Fig. 9). It should be mentioned that the Nusselt number for the second triangle in staggered arrangement is greater than the first triangle. It is because the channel becomes narrow by the presence of the first triangle, and it causes the flow to accelerate. The total Nusselt number for in-line arrangement is shown in Fig. 17 for comparison with the staggered arrangement (Fig. 16).

6. Conclusion

The effect of longitudinal and lateral gap between two isothermal staggered triangular cylinders on fluid flow and heat transfer is investigated numerically in a horizontal plane channel. The main results are summarized as follows:

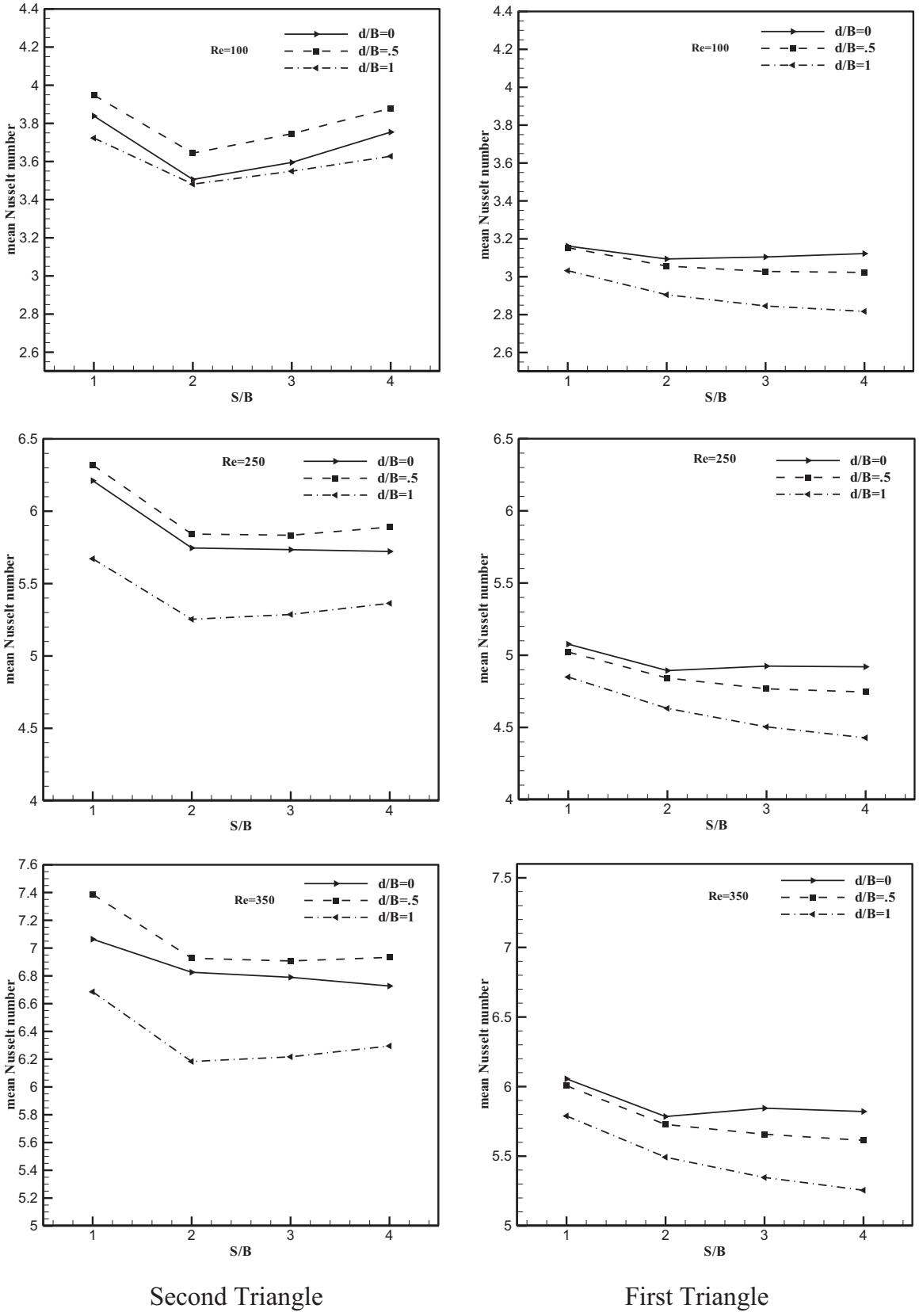

Fig. 16. Variation of total time-averaged Nusselt number versus longitudinal gap ratio (S/B) at different lateral gap ratio (d/B) for staggered arrangement.

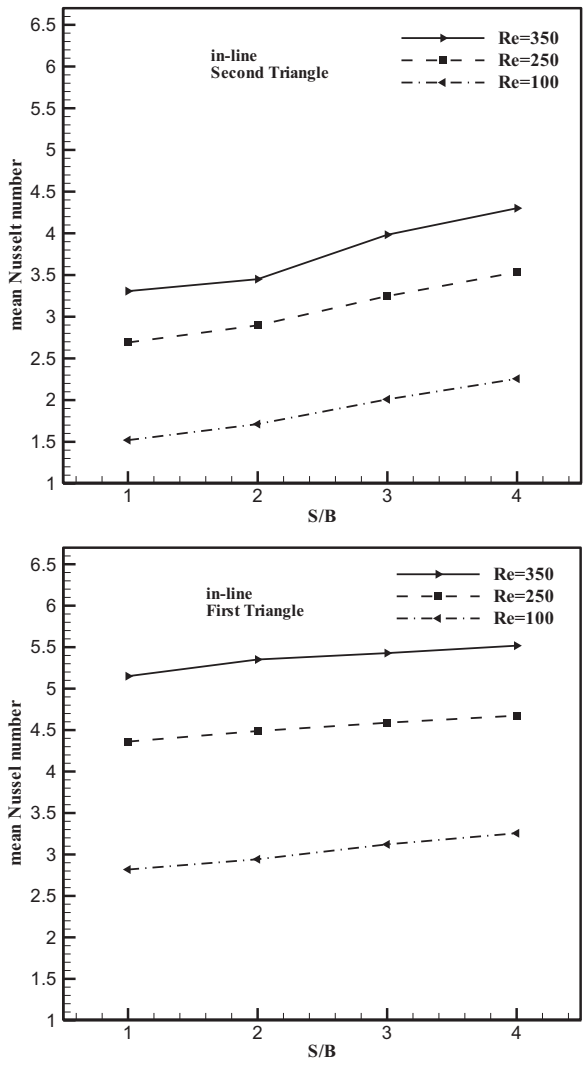

Fig. 17. Variation of total time-averaged Nusselt number versus longitudinal gap ratio (S/B) at different Reynolds number for in-line arrangement.

- At S/B = 1, drag coefficient of both obstacle at d/B = 0 is smaller than other lateral gap ratio (d/B = 0.5, 1), but with increasing S/B it starts to become greater than other lateral gap ratio.
- At all longitudinal gap ratio (S/B = 1 to 4), with approaching the wall at d/B = 1, vortex shedding disappears downstream of both obstacles at Re = 100, 250. But for Re = 350, with increasing longitudinal gap ratio, S/B, a different behavior is seen in d/B = 1.
- With approaching the wall, Nusselt number of the first triangle decreases at all S/B.
- Nusselt number of the second triangle is greater than the first triangle.
- Proximity of two triangles has more effect on the second triangle than the first triangle, because of the following:
  - ü Drag coefficient of the first triangle at d/B = 0 from S/B = 2 onwards becomes greater than other lateral space (d/B = 0.5, 1), but for the second triangle it happens from S/B = 3 onwards.
  - ü Nusselt number of the second triangle at d/B = 0.5 is greater than the other lateral gap ratio (d/B = 0, 1) while for the first triangle it is the greatest at d/B = 0.

Nomenclature

B	Triangle width, m
C_d	Drag coefficient, $=FD/(0.5\rho_a u_{max}{}^2 A)$
C_p	Pressure coefficient, $=(P^* - P^*_0)/(0.5\rho_a u_{max}{}^2)$
d	Lateral gap space between triangular cylinder, m
d/B	Lateral gap ratio
f	Eddy-shedding frequency
H	Channel width, m
h	Half of the channel width, =H/2, m
Nu	Local Nusselt number, $=-\partial\theta/\partial n\big\vert_{n=0}$
$\overline{Nu}$	Streamwise averaged Nusselt number
<Nu>	Time-averaged Nusselt number
$\langle\overline{Nu}\rangle$	Streamwise and time-averaged Nusselt number
p^*	Pressure, Pa
p	Dimensionless pressure, $=\left(P^*/\rho u_{max}^2\right)$
Pr	Prandtl number, $=(\nu/\alpha)$
Re	Reynolds number, $=(u^*_{max}B/\nu)$
S	Longitudinal gap space between triangles, m
S/B	Longitudinal gap ratio
Sr	Strouhal number, $=(fB/u^*_{max})$
T	Temperature, K
t	Time, s
(u^*,v^*)	Velocity components, ms^{-1}
u^*_{max}	Maximum of u^* components at the channel inlet, ms^{-1}
(u, v)	Dimensionless velocity, $=(u^*,v^*)/u^*_{max}$
(x^*, y^*)	Cartesian coordinates, m
(x,y)	Dimensionless coordinates, $=(x^*,y^*)/B$

Greek symbols

τ	Dimensionless time, $=(tu^*_{max}/B)$
θ	Dimensionless temperature, $=(T - T_C)/(T_H - T_C)$
ν	Kinematics viscosity, m^2s^{-1}

Subscripts

C	Cold
H	Hot

References

[1] J.J. Wang, P.F. Zhang, S.F. Lu, K. Wu, Drag reduction of a circular cylinder using an upstream rod, Flow Turbul. Combust. 76 (2006) 83–101.
[2] P.F. Zhang, J.J. Wang, S.F. Lu, J. Mi, Aerodynamic characteristics of a square cylinder with a rod in a staggered arrangement, Exp. Fluids 38 (2005) 494–502.
[3] M. Molki, D. Fotouhi, Thermal field around a circular cylinder with periodic vortex shedding, Int. J. Eng. 10 (1) (1997) 27–36.
[4] D. Sumner, M.D. Richards, O.O. Akosile, Two staggered circular cylinders of equal diameter in cross-flow, J. Fluid Struct. 20 (2005) 255–276.
[5] P. Dey, A.K. Das, Numerical analysis of drag and lift reduction of square cylinder, Eng. Sci .Technol. 18 (4) (2015) 758–768.
[6] M.H. Akbari, S.J. Price, Numerical investigation of flow patterns for staggered cylinder pairs in cross-flow, J. Fluids Struct. 20 (2005) 533–554.
[7] R.S. Matos, T.A. Laursen, J.V.C. Vargas, A. Bejan, Three-dimensional optimization of staggered finned circular and elliptic tubes in forced convection, Int. J. Therm. Sci. 43 (2004) 477–487.
[8] R.D. Ghosh, S.K. Das, T. Sundararajan, Numerical simulation of laminar flow and heat transfer over banks of staggered cylinders, Int. J. Numer. Methods Fluids 39 (2002) 23–40.
[9] H. Hasanzadeh Afrouzi, K. Sedighi, M. Farhadi, E. Fattahi, Dispersion and deposition of micro particles over two square obstacles in a channel via hybrid lattice Boltzmann method and discrete phase model, Int. J. Eng. 25 (3) (2012) 257–266.
[10] G. Buresti, G. Lombardi, A. Talamelli, Low aspect-ratio triangular prisms in cross-flow: measurements of the wake fluctuating velocity field, J. Wind Eng. Ind. Aerodyn. 74–76 (1998) 463–473.
[11] A.L. Csiba, R.J. Martinuzzi, Investigation of bluff body asymmetry on the properties of vortex shedding, J. Wind Eng. Ind. Aerodyn. 96 (6–7) (2007) 1152–1163.
[12] E. Ulrichs, H. Herwig, Between two limits: flow separation behind a bluff body close to a wall, Forschung im Ingenieurwesen 68 (2003) 36–38.
[13] S. Camarri, M.V. Salvetti, G. Buresti, Large-eddy simulation of the flow around a triangular prism with moderate aspect ratio, J. Wind Eng. Ind. Aerodyn. 94 (5) (2006) 309–322.
[14] H. Abbassi, S. Turki, S. Ben Nasrallah, Numerical investigation of forced convection in a plane channel with a built-in triangular prism, Int. J. Therm. Sci. 40 (2001) 649–658.

[15] H. Chattopadhyay, Augmentation of heat transfer in a channel using a triangular prism, Int. J. Therm. Sci. 46 (2007) 501–505.
[16] S. Fohanno, G. Polidori, Effect of the gap size in the start-up free convective flow around a square prism near a wall, Int. J. Heat Fluid Flow 26 (2005) 25–33.
[17] S. Wang, L. Zhu, X. Zhang, G. He, Flow past two freely rotatable triangular cylinders in tandem arrangement, J. Fluids Eng. 133 (8) (2011) 81202–81213.
[18] J. Tu, D. Zhou, Y. Bao, Z. Han, R. Li, Flow characteristics and flow-induced forces of a stationary and rotating triangular cylinder with different incidence angles at low Reynolds numbers, J. Fluids Struct. 45 (2014) 107–123.
[19] S. Ghafouri, M. Alizadeh, S.M. Seyyedi, H. Hassanzadeh Afrouzi, D.D. Ganji, Deposition and dispersion of aerosols over triangular cylinders in a two-dimensional channel; effect of cylinder location and arrangement, J. Mol. Liq. 206 (2015) 228–238.
[20] N. Agrwal, S. Dutta, B.K. Gandhi, Experimental investigation of flow field behind triangular prisms at intermediate Reynolds number with different apex angles, Exp. Therm. Fluid Sci. 72 (2016) 97–111.
[21] D.F.G. Durao, P.S.T. Gouveia, J.C.F. Pereira, Velocity characteristics of the flow around a square cross-section cylinder placed near a channel wall, Exp. Fluids 11 (1991) 298–304.
[22] G. Bosch, M. Kappler, V. Rodi, Experiments on the flow past a square cylinder placed near a wall, Exp. Therm. Fluid Sci. 13 (1996) 292–305.
[23] C. Lei, L. Cheng, K. Kavanagh, Re-examination of the effect of a plane boundary on force and vortex shedding of a circular cylinder, J. Wind Eng. Ind. Aerodyn. 80 (1999) 263–286.
[24] A.J. Grass, P.W.J. Raven, R.J. Stuart, J.A. Bray, The influence of boundary layer velocity gradients and bed proximity on vortex shedding from free spanning pipelines, J. Energy Resour. Technol. 106 (1984) 70–78.
[25] D. Chakrabarty, R. Brahma, Effect of wall proximity in fluid flow and heat transfer from a square prism placed inside a wind tunnel, Therm. Sci. 11 (2007) 65–78.
[26] D. Chakrabarty, R.K. Brahma, Effect of wall proximity in fluid flow and heat transfer from a rectangular prism placed inside a wind tunnel, Int. J. Heat Mass Transf. 51 (2008) 736–746.
[27] A.K. Singha, A. Sarkar, P.K. De, Numerical study on heat transfer and fluid flow past a circular cylinder in the vicinity of a plane wall, Numer. Heat Transf. A Appl. 53 (2008) 641–666.
[28] J.L. Rosales, A. Ortega, J.A.C. Humphrey, A numerical simulation of the convective heat transfer in confined channel flow past square cylinders: comparison of in-line and offset tandem pairs, Int. J. Heat Mass Transf. 44 (2001) 587–603.
[29] A. Mohsenzadeh, M. Farhadi, K. Sedighi, Convective cooling of tandem heated triangular cylinders confined in a channel, Therm. Sci. 14 (2010) 183–197.
[30] M. Farhadi, K. Sedighi, A. Mohsenzadeh Korayem, Effect of wall proximity on forced convection in a plane channel with a built-in triangular cylinder, Int. J. Therm. Sci. 49 (2010) 1010–1018.
[31] S. Srikanth, A.K. Dhiman, S. Bijjam, Confined flow and heat transfer across a triangular cylinder in a channel, Int. J. Therm. Sci. 49 (2010) 2191–2200.
[32] M. Ali, O. Zeitoun, A. Nuhait, Forced convection heat transfer over horizontal triangular cylinder in cross flow, Int. J. Therm. Sci. 50 (2011) 106–114.
[33] O. Zeitoun, M. Ali, A. Nuhait, Convective heat transfer around a triangular cylinder in an air cross flow, Int. J. Therm. Sci. 50 (2011) 1685–1697.
[34] H. Ferziger Joel, M. Peric, Computational Methods for Fluid Dynamics, third ed., Springer-Verlag, Berlin Heidelberg, 2002.
[35] A. Sohankar, C. Norberg, L. Davidson, Low-Reynolds number flow around a square cylinder at incidence: study of blockage, onset of vortex shedding and outlet boundary condition, Int. J. Numer. Methods Fluids 26 (1998) 39–56.